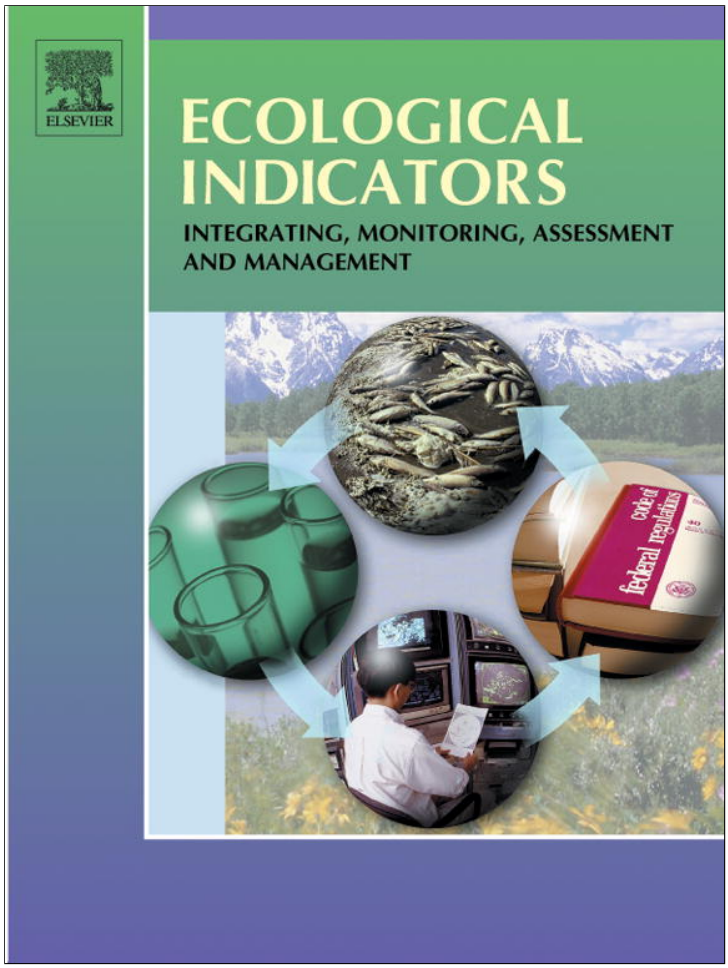

(This is a sample cover image for this issue. The actual cover is not yet available at this time.)

Ecological Indicators 27 (2013) 17–28

Contents lists available at SciVerse ScienceDirect

Ecological Indicators

journal homepage: www.elsevier.com/locate/ecolind

Ecosystem functional units characterized by satellite observed phenology and productivity gradients: A case study for Europe

E. Ivits*, M. Cherlet, W. Mehl, S. Sommer

Land Resource Management Unit, EC Joint Research Centre (JRC), Via E. Fermi 1, 21020 Ispra (VA) Italy

ARTICLE INFO

Article history:
Received 12 April 2012
Received in revised form 8 November 2012
Accepted 13 November 2012

Keywords:
Ecosystem functional units
Remote sensing
Phenology
Productivity
Gradient analysis
CART

ABSTRACT

The present study demonstrates remote sensing derived phenological and productivity indicators of ecosystem functional dynamism. The indices were derived from SPOT VEGETATION NDVI data on 1 km spatial resolution across the pan-European continent using the Phenolo approach. The phenological and productivity indices explained 78% of the variance in the European ecosystem gradient measured by bio-climatic zones. Along this gradient climatic predictors could only explain 57% of the variance in the satellite metrics. Reclassification of the bio-climatic zones into phenology and productivity related ecosystem functional units (EFUs) selected five metrics related to the cyclic and permanent fraction of productivity, to the background, to the growing season start and the timing of the maximum NDVI value. Along the EFU gradient the climatic predictors explained over 90% of the variance of the remote sensing variables, 30% more than along the bio-climatic gradient. The EFUs showed strong correspondence to 14 land-cover types in Europe and the selected remote sensing metrics explained 86% of the variation in the land-cover classes. These results show that remote sensing derived parameters have tremendous potential for the quantification of ecosystem functional dynamism. Phenological and productivity metrics offer an indicator system for ecosystems that climatic indicators alone cannot manifest. Their potential to monitor the spatial pattern, status and inter-annual variability of ecosystems and vegetation cover can deliver reference status information for future assessments of the impacts of human or climate change induced ecosystem changes.

1. Introduction

There is growing evidence that global environmental degradation is largely due to intensive human use together with increasing awareness of the dependence of people on the Globe's ecosystem services (Ayensu et al., 1999). Ecosystem degradation arise from long lasting loss of vegetation cover and biomass productivity over time and in space (Hellden and Tottrup, 2008) resulting from a combination of natural and socio-economic drivers. The intense over-exploitation of certain ecosystem services (such as food, fibre, etc.) is one of the major drivers leading to degradation of the environment and can cause an irreversible loss of e.g. the supporting ecosystem services (Hill et al., 2008). In this context intensive land-use and land-use change is a major driver and indicator of ecosystem change (Lambin and Geist, 2006) that might lead to the degradation of lands and supporting services. Still little is known of the current state and future prospects of these services (Ayensu et al., 1999) and their complex interactions call for a coherent approach to understand the coupled human-environment system (Millenium Ecosystem Assessment, 2005). The need for improved information on the status of ecosystems and on their ongoing degradation, along with properly agreed up-to-date, effective and repeatable methodologies and understandable mapping on large spatial scales has to be addressed urgently.

Ecosystems may be characterized based on the spatial distribution of the vegetation cover. The vegetation cover in turn can be basically described by three measures: physiognomy, dynamics and taxonomy, whereas the latter has smaller importance when functional dynamisms are of interest (Graetz, 1989). Physiognomy and dynamics deal with vegetation phenology and its change in space and time stressing on the importance of large scale, spatially continuous and repeatable assessment methods. Monitoring vegetation phenology is crucial for estimating productivity of lands (Keeling et al., 1996) and is essential for understanding the interactions between the biosphere, the climate and biogeochemical cycles (Myneni et al., 1997; Schwartz and Reed, 1999; Menzel, 2000; Nemani et al., 2003). Furthermore, vegetation distribution is associated with climate, terrain characteristics and human activity (Azzali and Menenti, 2000) thus monitoring systems may enable the assessment of these factors as well. A useful monitoring system therefore supplies indicators that address the climate dependence of vegetation phenology, is responsive to land cover and land use

* Corresponding author. Tel.: +39 0332 78 5315.
E-mail address: eva.ivits-wasser@ext.jrc.ec.europa.eu (E. Ivits).

1470-160X/$ – see front matter © 2012 Elsevier Ltd. All rights reserved.
http://dx.doi.org/10.1016/j.ecolind.2012.11.010

while supplying knowledge of the temporal and spatial patterns of ecosystem functioning at larger spatial scales. In this context, ecosystem functional types (EFTs, Paruelo et al., 2001; Alcaraz et al., 2006) offer an optimal framework for functional classification of ecosystems because they represent the spatial heterogeneity in ecosystem functioning and are related to land cover.

Although the merit of in situ observations is unquestionable, up-to-date only remote sensing can offer effective, repeatable and spatially explicit information on ecosystem phenology and productivity over several temporal scales and continuous spatial coverage. This is even more so because environmental changes are especially noticeable at the ecosystems level (Vitousek et al., 1997) and because in situ phenological data are comparatively scarce in many parts of the world (Chen and Pan, 2002). Several studies have used remote sensing observed phenological indices for the monitoring of vegetation dynamics from regional to global scales. Among others, Hogda et al. (2001) found a delay of spring in the alpine belts and the northern boreal zone during the period 1981–1998 whereas Zhou et al. (2001) found a comparable delay in the decline of autumn activity in Eurasia relative to North America. Julien and Sobrino (2009) showed global advance in spring dates of 0.38 days and a global increase of season length of 0.8 days per year. Zhu et al. (2011) and Jeong et al. (2011a) have observed that the prolonged length of the growing season over the mid and high latitudes of North America was due to delayed dormancy rather than to advanced greenup. Jeong et al. (2011b) noted earlier greenup in the Northern Hemisphere but delays when trends were observed on the continental scale. deBeurs and Henebry (2004) analyzed land surface phenology, climatic variation, and institutional change and showed that phenological changes are land cover dependent. Fensholt et al. (2012) showed an increase in greenness in semi-arid areas despite general concerns of land degradation in these regions. For Europe, Stöckli and Vidale (2004) showed an earlier and prolonged growing period for the years 1982–2001 whereas Ivits et al. (2012) analyzed the start and the length of the growing season over 25 years and mapped the spatial distribution of seasonal shifts. Studer et al. (2007) compared a multispecies index from ground-observed spring phases with satellite-derived start-of-season metrics for Switzerland showing good correlation and also good agreement with temperature anomalies.

The capability of remote sensing indicators to capture ecosystem functional dynamism has been a comparably neglected issue so far. Remote sensing derived vegetation phenology may provide an integrated measure of ecosystem responses to climatic factors such as temperature and rainfall as well as fire and other disturbances (Wessels et al., 2010). In this study we address ecosystem functional units (EFUs) as areas exhibiting similar responses to environmental conditions and similar ecosystem processes by calculating phenological and productivity metrics from time-series of remote sensing images over the pan-European continent. We show that EFUs contribute to classifications at the sub-biome level where variations in vegetation structure and function are driven by factors such as soils, topography, land-cover and land-use (Wessels et al., 2010). The relationship between satellite measured phenology and ecosystem can be highly site specific (White et al., 1997; Chen et al., 2001) and the degree of climatic controls varies with locations (Jolly and Running, 2004). Therefore we tested whether satellite derived phenological and productivity metrics are able to describe the spatial gradient of the European ecosystems in various bio-climatic zones. Seasonal temperature and precipitation data were acquired to test the magnitude of climate control over the satellite derived information and to quantify the variation that climate does not explain. The potential of phenological and productivity metrics was further exploited by demonstrating the association of the EFUs with continental scale bio-climatic gradients, climatic predictors and land cover.

2. Material and methods

2.1. Test site and data

We selected the pan-European continent as test site with various climatic and ecological zones, heterogeneous land cover and intensive land use. It comprises well documented and well known ecosystems that supposedly indicates human influence and thus aids quantifying the capacity of phenological and productivity variables as ecosystem indicators. The study region covers the area from 65°7′58.47″N and 37°46′47.12″W (upper left) to 23°24′38.59″N and 42°49′23.25″E (lower right). We chose the global environmental stratification (GEnS, Metzger et al., 2011) in order to supply the analysis with a spatial framework that is heterogeneous enough to capture such diverse ecosystems as the European continent and has higher spatial resolution than other coarse scale climatic classifications. The GEnS consists of 125 strata and 18 global environmental zones at a 30 arcsec resolution (equivalent to 0.86 km^2 at the equator). It is a consistent quantitative stratification of the land surface into relatively homogeneous bio-climatic strata. We selected the 9 environmental zones (that are referred to as “ecozones” hereafter) and the 72 environmental strata (hereafter “strata”) that were within the spatial extent of the study (Fig. 1).

Normalized Difference Vegetation Index (NDVI) data at a spatial resolution of 1 km × 1 km and a temporal resolution of 10 days were acquired from the SPOT VEGETATION sensor distributed and produced by Vito (http://free.vgt.vito.be/). These NDVI data are 10-day maximum-value composites where the highest NDVI is selected to represent the period that reduces negatively biased noise due to the interference of clouds and atmospheric constituents. Many studies employed NDVI data to tackle the effect of biosphere processes and land cover characterization, the estimations of land cover variables as well as the quantification of the mechanisms by which vegetation cover and ecosystems are interlinked (for an overview see Hill et al., 2008; Hellden and Tottrup, 2008). In the present study the time-series of NDVI data is used for the calculation of phenological and productivity indices in order to assess ecosystem dynamism. The time span of the data covered 1st of October 1998 to 31st of March 2011.

Land cover information was acquired from the Global Land Cover Classification (GlobCover2009) dataset on 1 km × 1 km spatial resolution (http://ionia1.esrin.esa.int/). Currently, GlobCover 2009 is the most detailed and recent global land cover map available with a hierarchic thematic legend consisting of 22 classes. For the present study we selected 13 land cover classes from the European coverage partly taking the original classes and partly regrouping them into categories that were expected to be reflected by remote sensing derived phenological and productivity variables (Table 1). For instance, it was not expected that phenological and productivity variables, which are indicative to the dynamism of the yearly vegetation cycle, would discriminate between closed or open forest cover or between broadleaved and needleleaved tree stands. These classes therefore were grouped into the evergreen, deciduous or mixed forest categories, respectively where the yearly phenological and productivity cycle is expected to show differences. The GlobCover 2009 classes covering regularly flooded areas were not represented in the study area.

Precipitation and minimum and maximum temperature data were acquired from the European Centre for Medium-Range Weather Forecast (ECMWF) global circulation model data at 10 daily intervals and at a 1° spatial resolution. For the subsequent analysis we calculated the seasonal average and the seasonal coefficient of variation of the minimum temperature (MinT), maximum temperature (MaxT) and precipitation (Prec) for the years 1999–2010. The season were defined as follows: winter for the months December–January–February, spring for the months

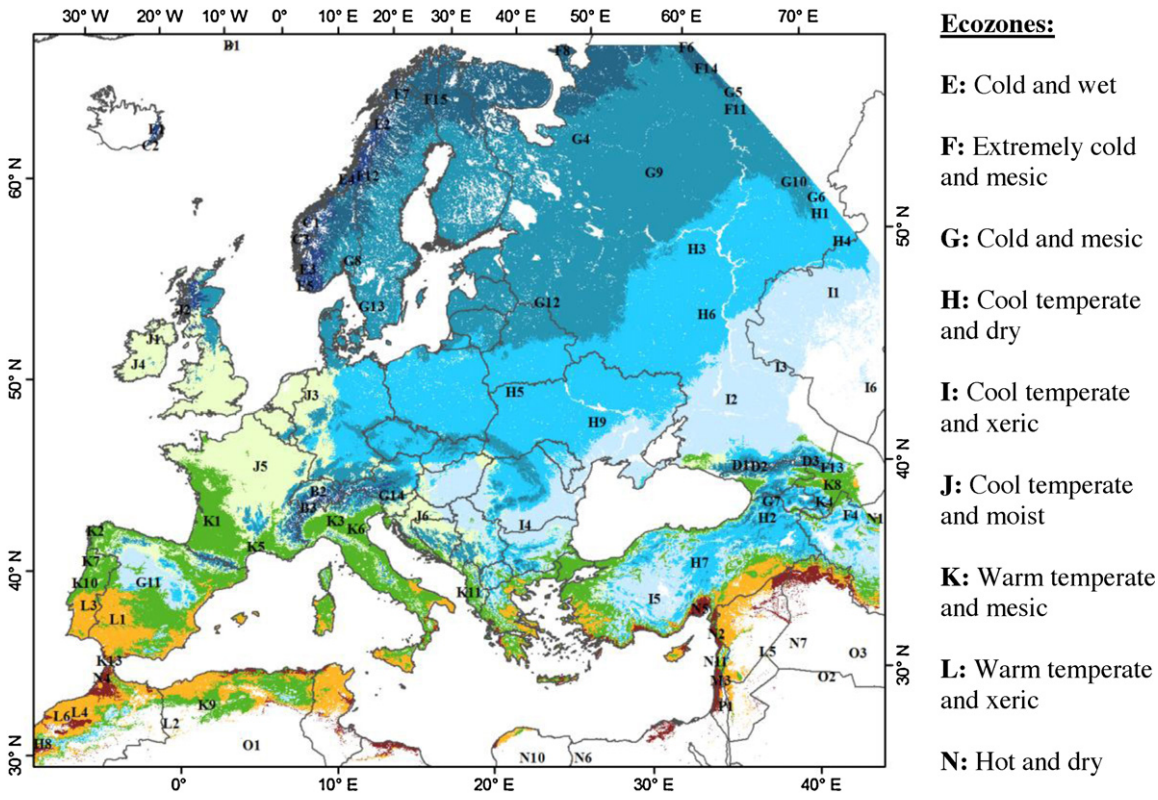

Fig. 1. European subset of the Global Environmental Classification with the nine ecozones (colours) and 73 strata (shown by numbered capital letters).

March–April–May, summer for the months June–July–August and autumn for the months September–October–November.

2.2. Derivation of phenological and productivity parameters: the Phenolo approach

Recently, the derivation of phenological parameters from time-series of remote sensing images has been given much attention (e.g. Reed et al., 1994; Zhang et al., 2003; Jönsson and Eklundh, 2004; Bradley et al., 2007). Most of these methods concentrate on the derivation of the start, the end and the maximum date of the vegetation growing season together with productivity measures approximating Net Primary Productivity and growing season productivity. However, for the characterization of ecosystem dynamism a more complete set of indicators is needed. Furthermore, for the applicability of the method on the continental to global scale setting thresholds adapted to local processes should be avoided. For this reason the "*Phenolo*" software was developed in-house at the EC Joint Research Centre that derives a fuller range of ecosystem dynamism indicators. The following gives a short description of the approach. Fig. 2 presents the most important steps in a flowchart.

Pixels with missing data in the NDVI time-series larger than a pre-defined value (GAP, here 2 decades) are flagged to indicate that the calculated phenological parameters are uncertain. Otherwise missing values in the time-series are replaced by a cubic spline interpolation. In order to generate results comparable between data sources with different time aggregation windows, daily values are calculated by an iterative linear interpolation of the NDVI time-series decades. Subsequently, a Savitzky–Golay filter with 4th polynomial degrees and a length of 50 days (settings can be adjusted) is applied to the time series in order to identify and remove short peaks and drop-offs caused by noise. This pre-processing results in the reference time-series on which the

Table 1
GlobCover 2009 classes and the categories used in the present study.

Selected class	Abbreviation	GlobCover 2009 class
Irrigated agriculture	IrrAgr	Post-flooding or irrigated croplands
Rainfed agriculture	RainfAgr	Rainfed croplands
Mosaic cropland	MosCrp	Mosaic cropland (50–70%)/vegetation (grassland, shrubland, forest) (20–50%)
Mosaic vegetation	MosVeg	Mosaic vegetation (grassland, shrubland, forest) (50–70%)/cropland (20–50%)
Evergreen forest	EvrgFrst	Closed (>40%) needleleaved evergreen forest (>5 m)
Deciduous forest	DecFrst	Closed (>40%) broadleaved deciduous forest (>5 m); Open (15–40%) needleleaved deciduous forest
Mixed forest	MxdFrst	Closed to open (>15%) broadleaved evergreen and/or semi-deciduous forest (>5 m); Closed to open (>15%) mixed broadleaved and needleleaved forest (>5 m)
Open forest	OpnFrst	Open (15–40%) needleleaved deciduous or evergreen forest (>5 m);
Mosaic forest	MosFrst	Mosaic Forest/Shrubland (50–70%)/Grassland (20–50
Mosaic grassland	MosGrs	Mosaic Grassland (50–70%)/Forest/Shrubland (20–50%) Closed to open (>15%) grassland
Shrubland	Shrbld	Closed to open (>15%) shrubland (<5 m)
Sparse vegetation	Sparse	Sparse (>15%) vegetation (woody vegetation, shrubs, grassland)
Wetlands	Wtlnd	Closed to open (>15%) vegetation (grassland, shrubland, woody vegetation) on regularly flooded or waterlogged soil – fresh, brackish or saline water

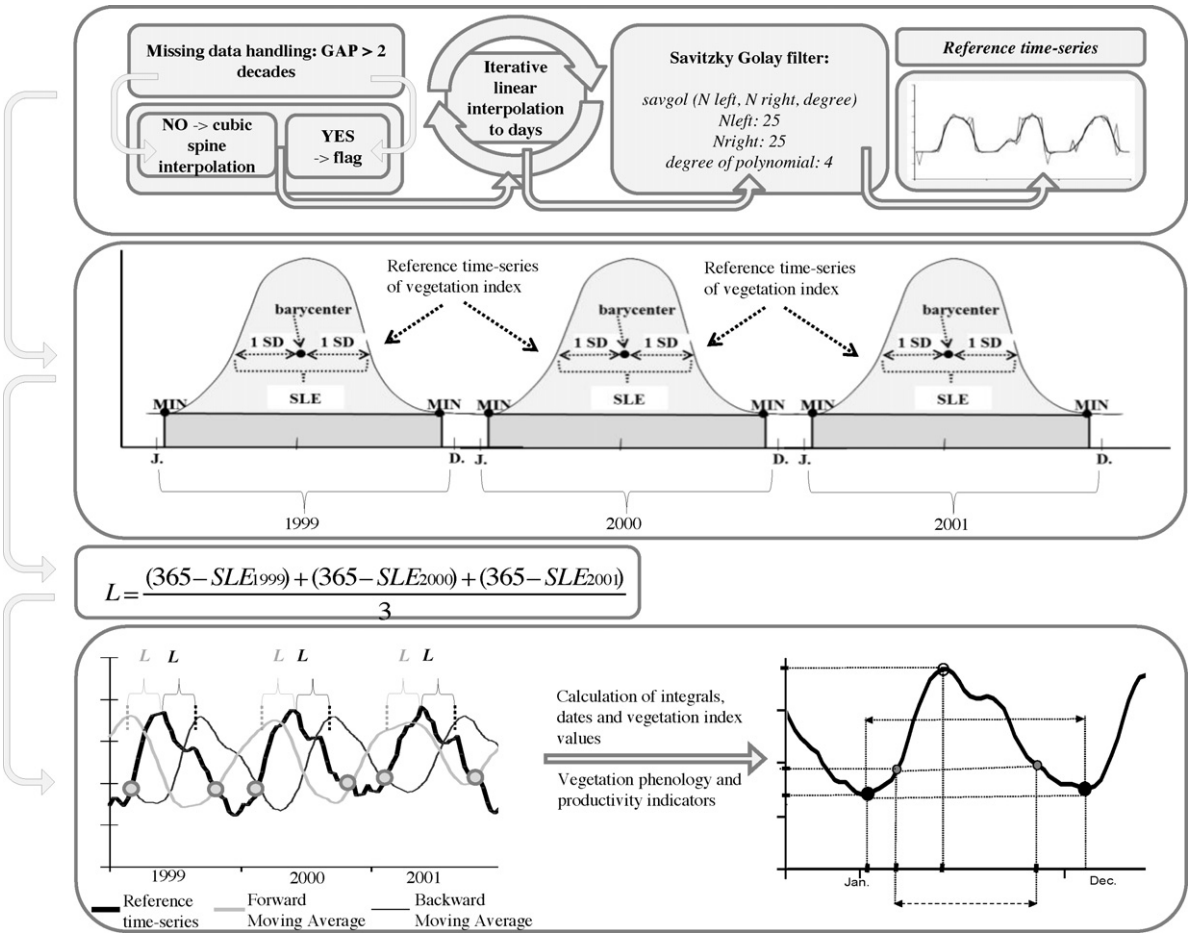

Fig. 2. A schematic representation of the main Phenolo processing steps for a time series composed of three years.

phenological parameters are to be computed. The methodology is based on computing a shifted and smoothed copies of the time-series using a moving average filter and extracting the intersection points of these with the reference time-series. While Reed et al. (1994) determined a general lag based on a priori knowledge about the average phenology of the study area, *Phenolo* is data driven using for each individual pixel its time series dynamism to determine the lag.

The lag (i.e. the size of the moving average window) is the estimated length of the non-growing season (*L*, see Eq. (1) and Fig. 2), defined for each pixel separately. *L* is derived based on a first approximation of the average growing season length (SLE) for the time-series of each pixel, as follows. For a given pixel and for a given year, between two subsequent NDVI signal minima the signal of the reference time-series above the line connecting the minima values (MIN, Fig. 2) is interpreted as a histogram, mean and standard deviation of which are determined. The obtained mean value is effectively passing through the barycentre (i.e. centre of mass) of the area delimited by the reference time-series and the baseline connecting the minima. By default, the SLE is defined to be two times the standard deviation (SD, expressed in days) computed from the barycentre of the area. Two standard deviations were taken as the default value because (1) it describes 68.2% of the statistical population with normal distribution, which can be considered a reasonable approximation of the shape of the time-series curve during the growing season and (2) with several test runs over nine bioclimatic zones it was proven appropriate (see supplementary material S1). SLE is computed for each year in the time series. The lag *L* is the yearly complement of SLE, where the yearly complement is calculated for each year and is averaged over the time-series:

$$L = \frac{\sum_{i=1}^{N}(365 - SLE)}{N} \quad (1)$$

where *L* is the lag (in days), *N* is the number of years in the time-series, SLE = 2 × SD and 365 is the number of days in the year.

This way the time series dynamism of each pixel is incorporated in the derivation of the phenological measures in an objective way, allowing the algorithm to be applied under broad geographical regions, land-use and ecosystems. Running the moving average filter in the forward direction (from the beginning to the end of the time series) results in a curve that lags behind the reference time-series whereas running the filter backward creates a forward lagging curve. The season begin day (SBD) and season end day (SED) are determined as the intersections of the reference time-series and the forward and backward lagged curves, respectively (Fig. 2, bottom). Once the above data points are determined, a number of additional parameters can be computed which may allow to trace characteristics of the vegetation cover and their respective changes over time (Fig. 3). All parameters relating to the timing of phenological events are expressed in days as explained above. Furthermore, values such as SBV, MXV, etc. are reported in percentage of the original NDVI scale (typically [−1; 1]) again to ease comparison between different sensors and products.

Note that the data points SBD and SED cannot always be determined unambiguously. Determination fails when there is no

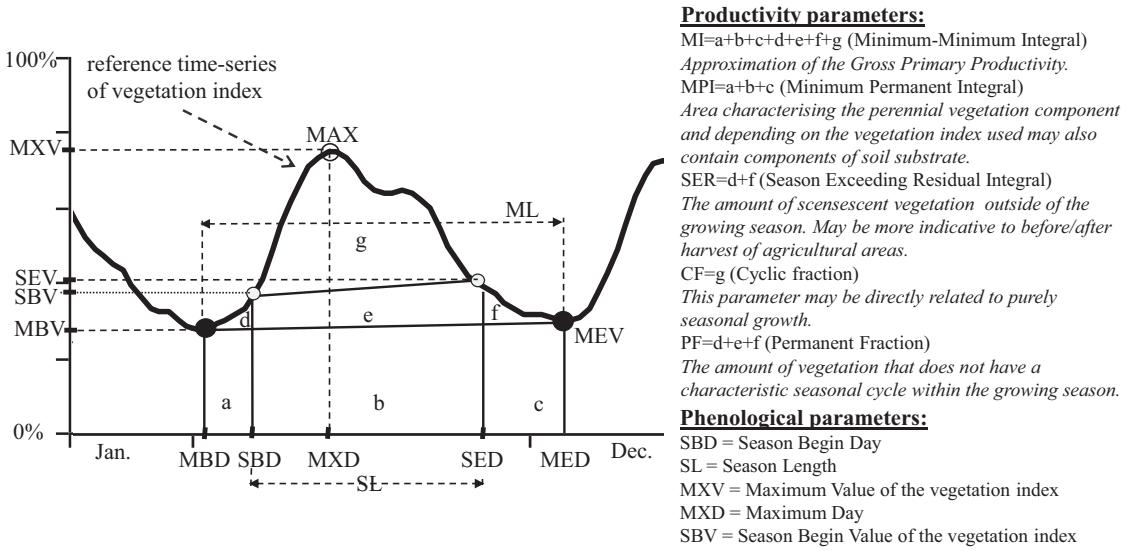

Fig. 3. Schematic representation of the phenological and productivity variables calculated by Phenolo. Phenolo calculates all the areas under the time-series curve and all time and value of the designed points. In the present study only the most important parameters were employed explained on the left.

significant seasonal variation, either due to extremely low vegetation density or because the vegetation cover is not subject to seasonal variations. However, even the failure to determine these points allows deducing certain land cover characteristics. Fig. 4 presents the SPOT VEGETATION NDVI signal over rainfed arable land pixels for three ecozones (see Fig. 1) and the forward and backward lagged moving average curves which determine the SBD and SED points. The moving average curves adjust to the typical seasonality profile of each ecozone due to the lag which is shifted according to the time series dynamism of the bio-climatic region. The SBD point is not biased by false season starts as e.g. in the northern F ecozone in the year 2001 (might arise due to early snow melt and subsequent snow-fall) and the moving averages are not influenced by the strong inter-annual variability of NDVI minimums as e.g. in the H and L zones. The temporal profiles of all ecozones are presented in Supplementary data S1.

2.3. Statistical analyses

The productivity and phenological variables as in Fig. 3 were calculated for each of the twelve years (1999–2010) separately for the entire spatial extent in Fig. 1. Consecutively the temporal mean of the variables were derived to characterize the "status" of the ecosystems. In order to tackle inter-annual fluctuations and dynamism the coefficient of variation (CV) of the variables was derived, which is preferable when comparing datasets with different units. For phenological variables that indicate dates the standard deviation (SD) was used because Julian days are directly comparable. The pixel values of the twelve years average MI image were scaled between 0 and 1 with the formula:

$$\mathrm{MI}_{\mathrm{scaled}} = \left(\frac{\mathrm{MI}_i - \min}{\max - \min}\right), i = 0, 1, \ldots, n, \quad (2)$$

where $\mathrm{MI}_{\mathrm{scaled}}$ are the rescaled MI values between 0 and 1. MI_i, (i runs till all the pixels in the image) is the calculated total integral under the NDVI curve (Fig. 3) for each pixel, min is the absolute smallest and max is the absolute largest MI value. The values of the other productivity variables were scaled in proportion of $\mathrm{MI}_{\mathrm{scaled}}$ and are reported as the percentage of MI, i.e. the total biomass.

The remote sensing variables (see Fig. 3 for the selected variables) and the seasonal climatic variables (MinT, MaxT, Prec) were averaged within the 73 strata of the ecozones. Standardized principal components analysis (PCA) was run with the remote sensing data and the strata to reveal if the phenological and productivity variables can measure the gradient of the European ecozones. Redundancy analysis (RDA) was used to assess how much of the variance in the remote sensing dataset can be explained by the climate data. The significant climate variables were selected using a permutational forward procedure as proposed by Blanchet et al. (2008) based on two stopping criteria: (1) the alpha significance level (here set at 0.05), and (2) the adjusted coefficient of multiple determination calculated using all explanatory variables. Only significant variables ($p < 0.05$) were included in the final RDA model. The significance and F-value of the derived canonical axes were determined with Monte-Carlo permutation test with 999 permutations. Results were presented in a tri-plot with the strata, the

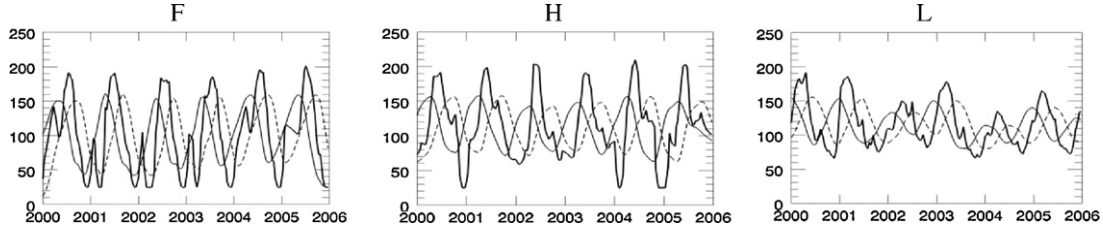

Fig. 4. SPOT Vegetation NDVI profiles (solid lines) and the moving average curves (dashed: backward MA, solid grey: forward MA) under rainfed arable land pixels in three ecozones in Europe (for the ecozones see Fig. 1). For clarity only the time interval 2000–2006 is plotted.

remote sensing variables and the climatic predictors. Based on the position of the environmental strata and the remote sensing variables one can infer the indicator value of the metrics for the ecozone. Strong correlation of the climate data and the RDA axes suggests that the gradient found within the environmental strata is climate driven. Arrows of the climate data and phenological variables pointing in the same direction indicate positive correlation.

A classification and regression tree (CART, Breiman et al., 1984) was run on the original pixel values in order to reclassify the ecozones into phenology and productivity driven EFUs. The pixel values rather than the values averaged within the environmental strata were used in order to supply a large statistical population for the analysis. The classification process was stopped after 5 classification levels reached. The tree was pruned in order to avoid overfitting with 1 standard deviation maximum difference allowed. The accuracy of each node was assessed by the Gini index, a variance estimate based on all comparisons of possible pairs of values in a subgroup. The Gini index also determined whether the node was a terminal node thereby stopping subsequent splits. The index is calculated as:

$$i(p) = 1 - \sum p^2(j|t), j = 1, 2, \ldots k, \quad (3)$$

where $p(j|t)$ is the probability distribution of a given ecozone in node t such that $p(1|t) + p(2|t) + p(3|t) + \ldots + p(k|t) = 1$. We defined the impurity of a tree over all terminal nodes to be the sum of the Gini index of the node multiplied by the proportion of cases that reached that node. We performed a split sample validation using a random assignment of 30% of the pixels as training sample and the remaining 70% as test sample. Classification accuracy and selected phenological and productivity variables are reported for the test sample. The importance of each predictor variable in relation to the final tree was defined as the (weighted) sum of the improvements across all splits in the tree that the variable had when it was used as a primary splitter.

The CART predictors and the climatic variables were averaged within the spatial units of the EFUs. A PCA was run to assess the variance that the remote sensing variables measured in the new environmental gradient defined by the EFUs. RDA was performed to measure the variance that the climate data explained in the remote sensing dataset along the new gradient. Finally, the EFUs were spatially intersected with the GLOBCOVER land cover dataset and the phenological and productivity classificators were averaged in each intersected unit. We evaluated the correspondence between the EFUs and the land cover classes through a correspondence analysis (CA) of the contingency matrix resulting from cross-tabulating the two dataset. Canonical correspondence analysis (CCA) was used on the GLOBCOVER classes to relate them to the selected remote sensing derived phenological and productivity measures within the EFUs.

3. Results

3.1. Bio-climatic gradient measured by remote sensing derived phenology and productivity

The first two PCA axes explained 56% and 22% of the variation in the ecozones, respectively, and together accounted for 78% (see variables in Fig. 5). The third and fourth axes were less important as they only explained 6% and 4% of the variation. RDA with forward selection chose five climatic variables that significantly ($p < 0.05$) explained the phenological and productivity variables across this gradient (Table 2). The inter-annual variation of summer (June–July–August) precipitation (PrecJJAs) was the strongest explanatory variable ($F = 43.3$; $p < 0.001$) followed by the mean winter (December–January–February) minimum temperature (MintDJFm, $F = 28.1$, $p < 0.001$). The climatic variables explained 57% variance in the remote sensing variables and the canonical axes were found significant by the Monte Carlo permutations (Appendix A, Table A1). The RDA axes also indicated two important environmental gradients.

The first RDA axis was identified as a strong gradient of the mean and of the inter-annual variation of the summer precipitation (inter-set correlation 0.849 and 0.865, respectively, Table 2) with a more moderate influence of the spring precipitation and of the minimum winter temperature. The RDA triplot (Fig. 5) shows that high summer precipitation and its high variation characterize the central and northern European regions whereas low precipitation together with high minimum winter temperatures describe the southern Mediterranean zones (L and N). The negative end of the first RDA axis correlated with the inter-annual variation of most of the remote sensing variables whereas the positive end correlated with the temporal mean of SL, MXV, SER, PF, MXD, CF and SBD. The second RDA axis emerged as a gradient from the North East regions (F, G and H zones) to the South-West and Atlantic (K and J zones) that correlated to the mean winter minimum temperature and the inter-annual variation of the spring precipitation. This axis showed strong positive correlation with the inter-annual variation of the season begin value and a strong negative correlation with the average background (MPI), SBV, and MI.

Strongest climate dependency was shown for the mean MXD which was explained to 87% by the climate data (Fig. 5). The maximum day was latest in the North Eastern F strata and the North Eastern part of the G and H zones. The mean CF and the SBD also showed high dependency on these climatic predictors over North Eastern Europe, they were explained to 83% and to 81% respectively. The mean SL was shown to be the least climate dependent variable as only 24% of its variation was explained by the climate data. The SL was shown to be the longest in the Atlantic J, in the surrounding G8–9 strata and in the Southern G11 strata. The RDA triplot indicated shortest SL in the Southern N and L zones. Climate explained only 33% of the variation in the inter-annual variation of the background, which showed high variation in South-Eastern I and L Strata. Furthermore, the climate data only explained 39% variation of the mean SER. This variable was the largest in the northern G zones and similarly to the SL showed lowest values in the Southern Mediterranean regions.

3.2. Classification of ecosystem functional units

The CART classification had an overall accuracy of 61% (Table 3) with an overall Gini impurity measure of 0.525. The classification tree did not assign the E and N zones, which were grouped together with the other environmental zones. The original 9 ecozones were reclassified into 19 ecosystem functional units (Fig. 6). The south-western intensively used J and K zones showed the lowest agreement with the EFUs whereas highest agreement was reached for the Northern H zone. The classification tree (Fig. 7) selected the temporal mean of five variables to reclassify the ecozones into 19 EFUs: MXDmn, PFmn, SBDmn, MPImn (background), and CFmn (see Supplementary material S3 for the spatial pattern of these variables). The PCA of the five remote sensing variables within the EFUs (Fig. 8) showed that the first four axes explained 99% of the variance, 10% higher than the bio-climatic classification of the ecozones. The first two PCA axes had the strongest explanatory value as together accounted for 88% variation (also 10% more than the original classification). The climatic predictors explained 90% of the variance in the remote sensing variables ($p < 0.001$) along the gradient of the EFUs, ca. 30% more compared to the gradient along the ecozones (see Appendix A, Table A2).

The mean permanent fraction separated the ecosystem functional units into (1) those with a PF less than 18% of the total

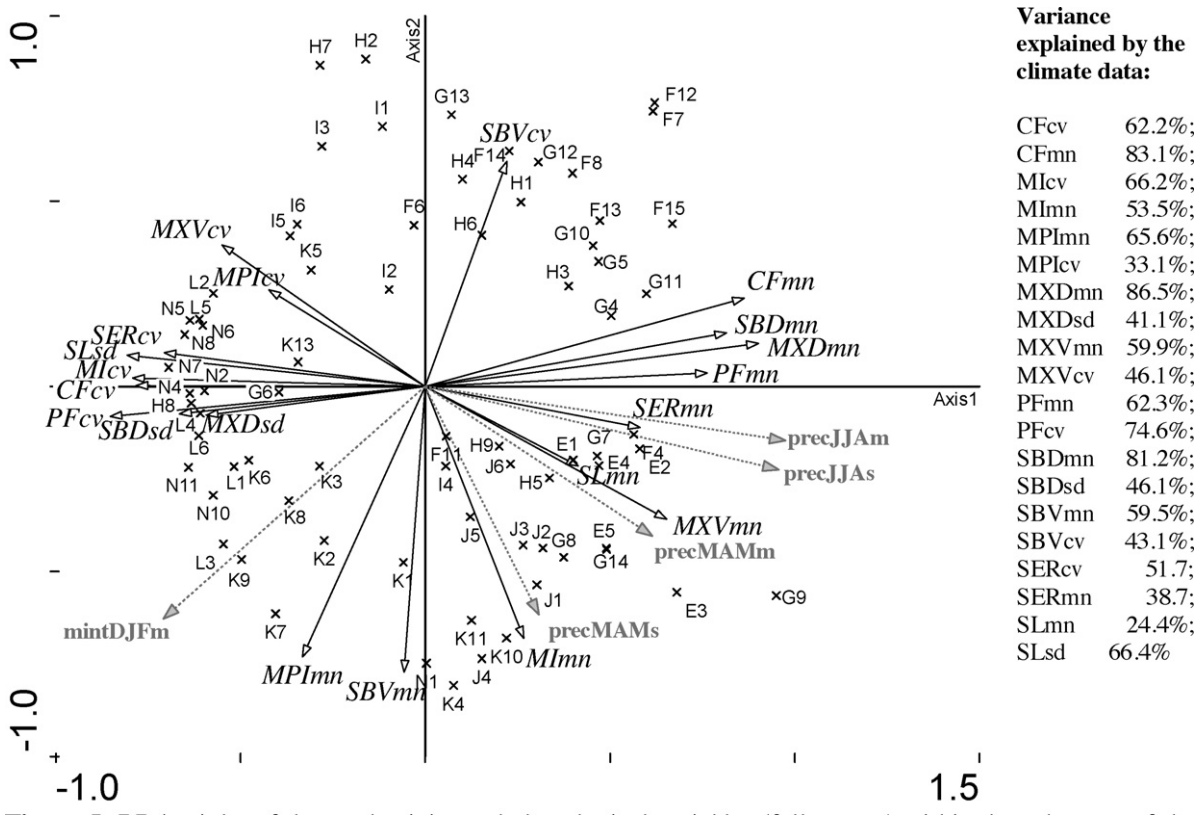

Fig. 5. RDA triplot of the productivity and phenological variables (full arrows) within the sub-strata of the ecozones (crosses with letters) with the forward selected climatic explanatory variables (dashed arrows).

Table 2
Forward selection of RDA: climate variables chosen by the adjusted R^2 values.

	R^2	Adjusted Cumulative R^2	*F*-value	*p*-value	Inter-set correlations with	
					RDA axis1	RDA axis2
MintDJFm	0.295	0.284	28.08	<0.001	−0.629	−0.459
PrecJJAs	0.279	0.561	43.34	<0.001	0.865	−0.107
PrecJJAm	0.058	0.616	10.42	<0.001	0.849	−0.164
PrecMAMm	0.027	0.639	5.19	=0.017	0.545	−0.295
PrecMAMs	0.044	0.682	9.50	=0.003	0.273	−0.541

biomass in Southern and Central Europe and into (2) those with a PF larger than 18% of the total biomass in the north-eastern G and H regions. These north-eastern regions were further characterized by high CF, which is also evident from the NDVI temporal profiles (Supplementary material S2). On the other hand, CF was only selected for the final classification of the Central Continental EFUs J3 (larger CF) and G5 (smaller CF), because both had large permanent fractions, late SBD, late MXD and large mean background. The Boreal G1 EFU had the largest PF and the largest CF (the latter is only evident from the PCA biplot, Fig. 8). MXD showed positive correlation to PF, CF and SBD over the northern regions indicating that these areas are characterized by late maximum, late start of season and by large permanent and cyclic fractions due to the relatively large amplitude of the NDVI signal over these areas (Sup-

Table 3
Contingency table and accuracy assessment of the EFUs classification using the remote sensing variables as predictors. Accuracy indicates the percentage of pixels in which the predicted category is the same as the observed category.

Observed	Predicted									Accuracy
	E	F	G	H	I	J	K	L	N	
E	0	58,825	45,528	40,993	4986	1714	235	1414	0	.0%
F	0	469,816	119,176	65,864	5809	216	233	1666	0	70.9%
G	0	116,693	1,860,892	976,322	60,952	53,535	435	123	0	60.6%
H	0	774	205,530	2,014,319	302,538	106,700	2588	1020	0	76.5%
I	0	21	15,402	286,868	1,194,528	64,472	30,289	6408	0	74.8%
J	0	0	21,565	418,588	49,715	513,366	50,230	886	0	48.7%
K	0	46	1404	157247	215269	324467	293733	82380	0	27.3%
L	0	50	833	18654	47055	11616	89761	384712	0	69.6%
N	0	17	1225	4520	9164	3981	23313	144212	0	.0%
Total accuracy:										61.3%

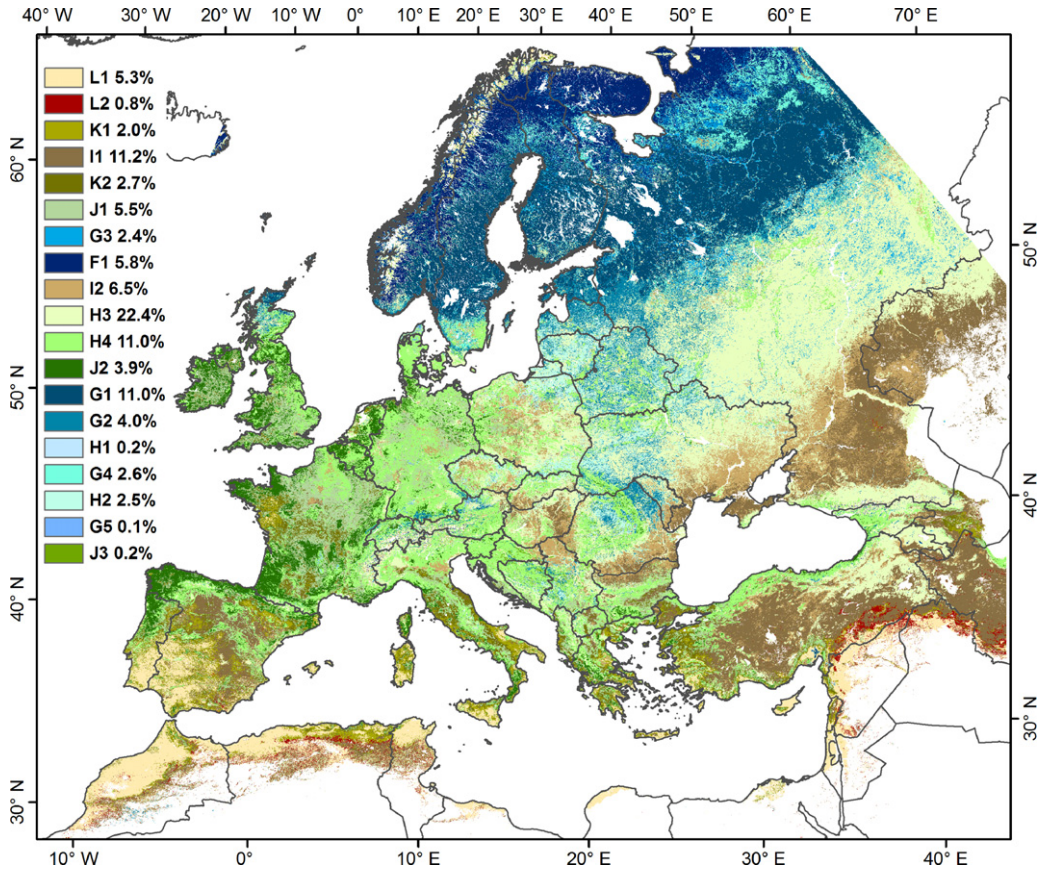

Fig. 6. Classification of the ecozones into ecosystem functional units with the remote sensing variables using thresholds from the classification tree. The values in the map show the EFUs' percentage in proportion of the study area.

plementary material S2). The F1 EFU in the circumpolar region and the G2 EFU in the Boreal region had the latest maximums. These regions were also characterized by latest SBD similarly to the J3 EFU.

SBD and MXD were earliest in the Mediterranean areas and accordingly these EFUs were plotted on the negative end of the first axis (Fig. 8). The vegetation maximum was the earliest in the L1 EFU (mid April) and in the L2 EFU (May, Figs. 7 and 8). These regions together with the K1 EFU had the smallest PF and CF also evident from the NDVI temporal profiles (Supplementary material S2). The K2 EFU of the northern Mediterranean had higher background (>25% of the total biomass) compared with the other Mediterranean areas (Figs. 6–8). Highest background, larger than 50% of the total biomass, was calculated for the J2 EFU situated over the North-West of the part Iberian Peninsula and the Western Atlantic regions. Figs. 6–8 and the NDVI temporal profiles (Supplementary material S2) indicated similar background, permanent and cyclic fractions for the geographically adjacent J2 and J1 EFUs in the Western Atlantic region but the PCA biplot shows that the maximum is reached earlier with earlier season start in the latter. The I2 EFU was plotted in the middle of the PCA biplot showing average phenological and productivity values due to the wide West-East geographic coverage of this zone.

3.3. Relation of the ecosystem functional units to land-cover

The ecosystem functional units showed very good correspondence with the GLOBCOVER land-cover classes as the first two CA axes accounted for 85% of the variation in the data. CCA indicated that the five phenological and productivity variables explained 86% of the variance in the land covers distributed in the EFUs with significant canonical axes (Appendix A, Table A3). The CCA triplot (Fig. 9) demonstrates the geographical correspondence of the land cover classes and the EFUs and their relation to the phenological and pro-

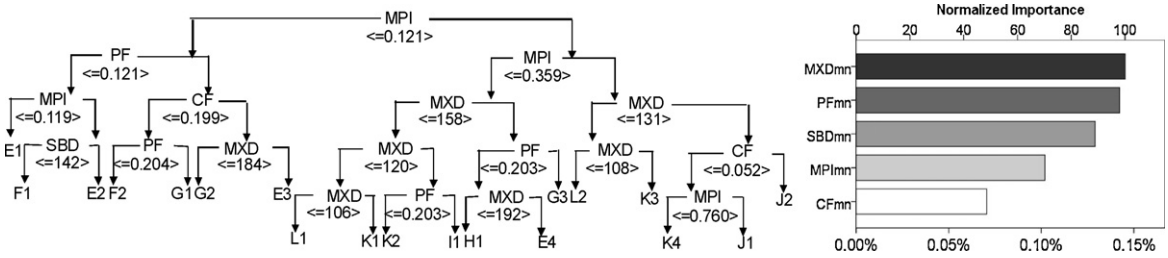

Fig. 7. Classification tree with the variable importance graph. Values in the tree indicate the splitting value of the given variable.

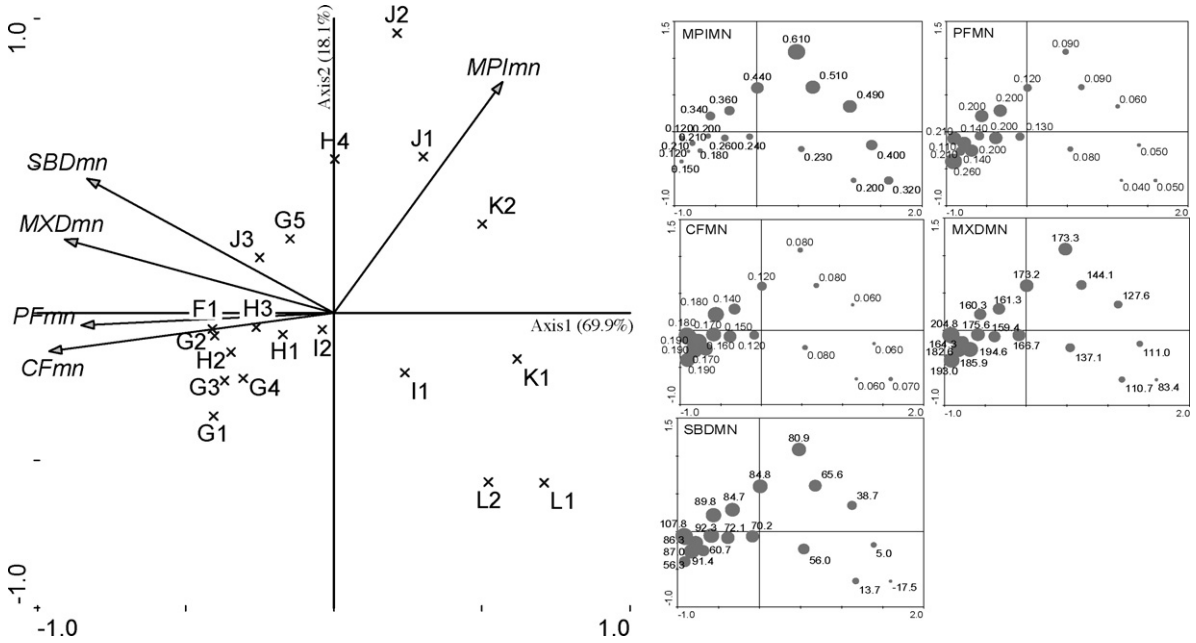

Fig. 8. PCA biplot of the productivity and phenological variables (arrows) selected for the reclassification of the ecozones into ecosystem functional units (crosses). Values along the axis show the percentage of explained variance. The diagrams show the average values of the remote sensing variables in the reclassified EFUs.

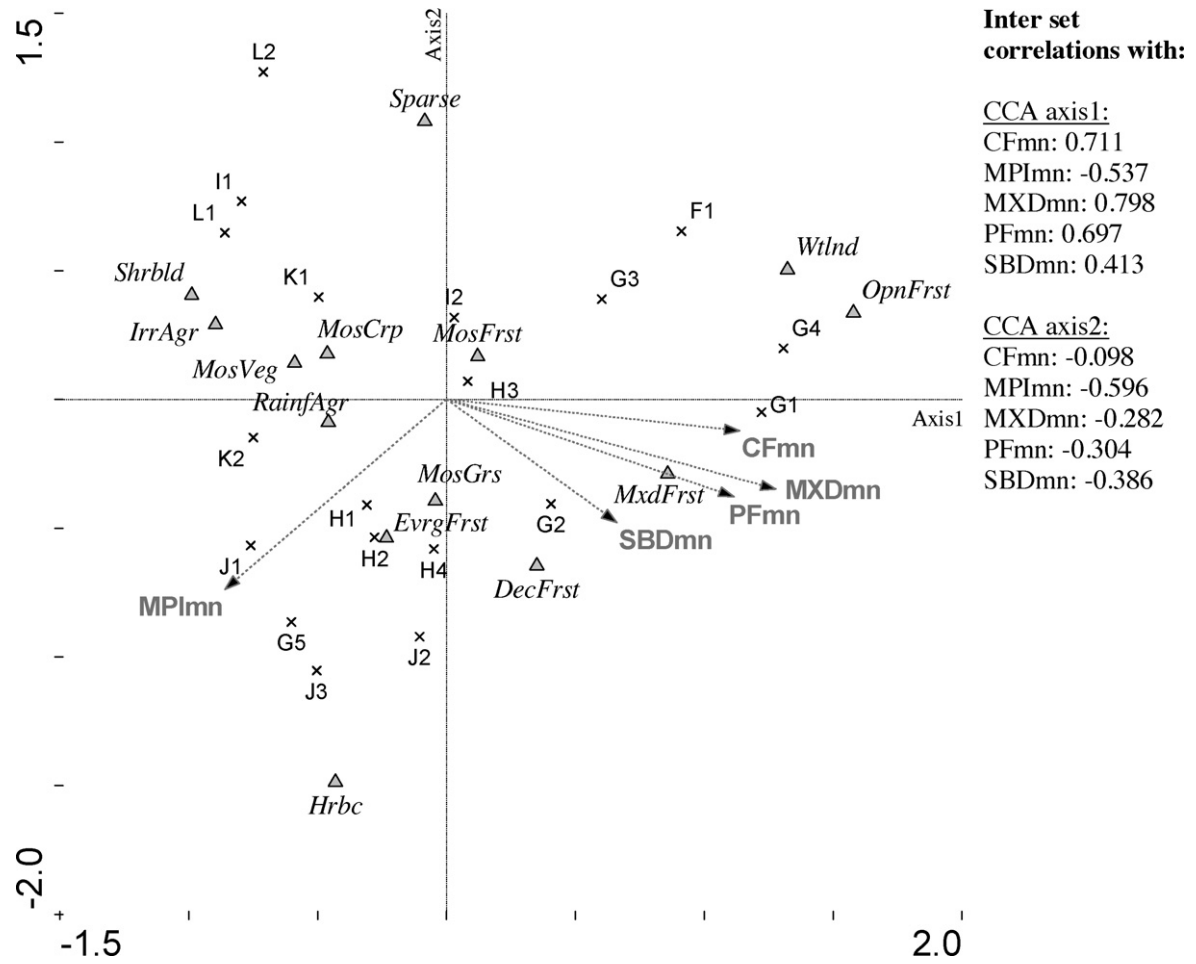

Fig. 9. CCA triplot of the GLOBCOVER classes (triangles) and the reclassified ecosystem functional units (crosses) with the remote sensing variables as predictors (dashed arrows). For the abbreviation of the land cover classes see Table 1.

ductivity variables. The mean CF and the timing of the maximum NDVI showed strongest association to the reclassified ecosystem gradient (inter-set correlations of 0.711 and 0.798, respectively, Fig. 9) along the first axis. Along the second axis the background was the most important predictor. The explanatory value of the SBD was comparably low.

Open needle-leaved forests, mixed forests and wetlands showed association to the northern F1 and Boreal G1, G3 and G4 ecosystem functional units with high PF, high CF and late maximum. Wetlands and open forests had the lowest background fractions. Deciduous forest was more associated to the Eastern European and Continental G2, H3 and H4 units with higher background, smaller PF and earlier NDVI maximums. Mosaic forest was plotted close to the centre of the biplot indicating close to average ecosystem phenology and productivity values. This land cover is a mixture of forests, grasslands and shrublands with wide occurrence over Europe thus the analysis could not place it onto either end of the gradient. Evergreen forest showed strong association to the continental H1, H2 and H4 EFUs with high background fraction and was distinguished from deciduous forest with earlier NDVI maximum and smaller CF and PF. Evergreen forest and mosaic grasslands could not be well distinguished based on their remote sensing derived phenology and productivity. Herbaceous vegetation in the Atlantic J1 and J2 and in the continental G5 and J3 units showed the highest background out of all land covers. Rainfed agriculture showed strong association with the mosaic cropland and mosaic vegetation land covers. These are widespread classes in Europe and accordingly they were not clearly associated with any of the EFUs. Irrigated agriculture on the other hand showed clear association with the southern European and Mediterranean units showing earlier season start, earlier maximum and lower CF and PF compared to rainfed agricultural areas. Shrubland showed similar phenology and productivity values to irrigated agriculture over the same regions. Sparse vegetation was associated to both the southern Mediterranean (L1, L2, I1) and the Northern F1 regions on two ends of the gradient with low background and low productivity values and with early season start and NDVI maximum.

4. Discussion and conclusions

PCA showed two strong environmental gradients in Europe captured by the ecozones and its strata. The first and stronger gradient mainly related to climatic influences and correlated with the mean and the inter-annual variation of summer precipitation with a more moderate influence of the spring precipitation and of the minimum winter temperature. Along this gradient the central and Northern European regions were characterized by high average PF and CF and phenological values correlating with high summer and spring precipitation. The southern European regions on the other hand were distinguished by highly fluctuating vegetation phenology and productivity related to low summer and spring precipitations. This complies with the general perception of phenology-climate dependency. The second RDA axis however showed only week correlation to climate and it emerged as a gradient from the North East zones with high inter-annual SBV variation to the South-West and Atlantic region with high background and high SBV. The climatic data could not explain 43% of the variance in the remote sensing derived parameters suggesting that productivity and phenological variables indicate a pattern in the European ecosystems gradient that climate alone cannot explain.

The strongest climate dependency of the mean MXD, SBD and CF (over 80%) confirms that the yearly cyclic dynamism of vegetation growth and the productivity of vegetation during this period are ecosystem functional indicators that are mostly dependent on seasonal precipitation and temperature patterns. Weakest climate dependency was shown for the mean SL and mean SER Integral and the inter-annual variation of the background, MXD, SBV and SBD also showed low correlation with the climate data. This suggests that these parameters capture ecosystems functional dynamisms that the climate data cannot manifest and are more related to other influencing factors like e.g. land use, management or soil characteristics. Indeed, short term variations in vegetation signals are not only driven by climatic cycles but among others, by management practices (Wessels et al., 2007). For example, harvest will characteristically cause earlier end of vegetation growing season and thus shorter season length as compared to natural areas. On the other hand, the season exceeding residual integral will be larger over natural areas compared to areas under management, because over the latter area the harvest removes most of this surface biomass. This underlines the importance of satellite derived phenology and productivity parameters as ecosystem change indicators because intensive management might result in irreversible loss of vegetation productivity that may lead to land degradation.

The agreement between the ecozones and the EFUs was 61% indicating that the remote sensing derived parameters contain ecosystem functional information that is not inherit in the bio-climatic strata as shown by the higher eigenvalues of the PCA calculated over the EFUs in comparison to the PCA over the ecozones. The climatic predictors explained over 90% of the variance of the remote sensing variables within the EFU's, 30% more than the variance explained within the bio-climatic zones suggesting that phenological and productivity parameters enhance the understanding and characterization of continental scale environmental gradients. The Western Atlantic J and Northern Mediterranean K ecozones were classified with the lowest accuracy whereas highest agreement was reached for the North-Eastern H ecozone. This shows that over the Northern regions vegetation phenology and productivity agrees with bioclimatic classification systems which are mostly dependent on climatic constraints. Over more intensively used and thus more fragmented landscapes however the remote sensing variables play a more important role in describing the spatial variability of vegetation cover due to (1) their higher spatial resolution and (2) differences in the functional dynamism inherit in the phenological and productivity indicators underlying the suitability of the remote sensing derived variables for improving ecosystem classifications. However, it must be noted that the classification tree could not discriminate the northern E and the southern N ecozones probably due to the similar phenological and productivity dynamism of these areas with the surrounding regions.

Our study also showed the suitability of remote sensing derived phenological and productivity parameters in indicating differences in land covers. CA indicated that 85% of the variation in the land covers was explained by the EFUs which is very high considering the different nature of the two datasets. For instance, irrigated agriculture showed earlier season start and earlier maximum together with lower cyclic and permanent fraction and thus could be clearly separated from rainfed agricultural areas. Also evergreen forest could be separated from deciduous forest with earlier NDVI maximum and smaller cyclic and permanent fractions. The mosaic forest class on the other hand, which is a mixture of forests/grasslands (50–70%) and shrublands (20–50%) with wide geographical occurrence over Europe could not be clearly assigned to either end of the ecosystem gradient that the EFUs represented. The EFUs classification agrees with climate driven gradients across the continent whereas in the GLOBCOVER classification the land cover classes are assigned irrespectively of the geographical setting of the ecosystems. These results show that remote sensing derived

phenological and productivity parameters have a large potential in improving classifications that mostly rely on the spectral properties of the land covers because the functional information inherit in them supply additional details on the dynamism of these land covers.

There is an urgent need for providing up-to-date, effective and repeatable indicator systems on large spatial scales for the monitoring and characterization of ecosystems. Mapping efforts that rely heavily on in situ data are time and resources consuming to update when ecosystems change due to climatic disturbances on the long term or due to droughts, floods, fires and human impacts on the shorter terms. Such maps cannot be used as real time information on the state of ecosystems and they are even less appropriate for mapping on regional, continental or local scales. The here presented phenological and productivity metrics were shown to (1) indicate the continental ecosystems gradient of Europe, (2) correlate with climate and (3) describe part of the spatial gradient that climate data could not. Incorporating the spatial information of these metrics into a new classification map delivered a stronger ecosystem gradient that was shown to be significantly related to land covers. Remote sensing derived vegetation phenological and productivity indicators can capture the spatial patterns of vegetation dynamics repetitively over vast areas (Jönsson and Eklundh, 2004), are directly related to key aspects of vegetation dynamism such as seasonality, productivity and inter-annual variation (Nemani et al., 2003) and have a tremendous potential for the monitoring of the status and change of ecosystems. The proposed set also has the ability of describing retrospectively properties of ecosystems functional units, and as further area of research it could be potentially exploited to support the quantification of ecosystems' properties as well as socio-ecological dynamics (Zaccarelli et al., 2008). These indicators offer a solid and effective set for the monitoring of the spatial pattern, status and inter-annual variability of ecosystems and have a potential to deliver reference status information for future assessments of the impacts of human or climate change induced ecosystem degradation.

Appendix A.

Tables A1–A3.

Table A1
RDA of the productivity and phenological variables with the climate data as predictors within the ecozones.

	AX1	AX2	AX3	AX4
Eigenvalues	0.418	0.124	0.018	0.008
Cumulative explained variance (%)	41.8	54.3	56.2	56.9
Sum of all canonical eigenvalues			0.572	
Significance of canonical axes (Monte Carlo permutation)			$p < 0.001$	
F-value			17.897	

Table A2
RDA of the productivity and phenological variables with the climate data as predictors within the ecosystem functional units.

	AX1	AX2	AX3	AX4
Eigenvalues	0.680	0.168	0.046	0.010
Cumulative explained variance (%)	68.0	84.8	89.4	90.5
Sum of all canonical eigenvalues		0.905		
Significance of canonical axes (Monte Carlo permutation)		$p < 0.001$		
F-value		24.643		

Table A3
CCA of the GLOBCOVER classes within the ecosystem functional units with the productivity and phenological variables as predictors.

	AX1	AX2	AX3	AX4
Eigenvalues	0.200	0.085	0.022	0.006
Cumulative explained variance (%)	54.8	78.1	84.1	85.7
SE: Sum of all eigenvalues		0.366		
SCE: Sum of all canonical eigenvalues		0.316		
Variance explained by the predictors:		(SCE/SE) × 100 = 86.3%		
Significance of canonical axes (Monte Carlo permutation)		$p < 0.001$		
F-value		16.746		

Appendix B. Supplementary data

Supplementary data associated with this article can be found, in the online version, at http://dx.doi.org/10.1016/j.ecolind.2012.11.010.

References

Alcaraz, D., Paruelo, J., Cabello, J., 2006. Identification of current ecosystem functional types in the Iberian Peninsula. Global Ecol. Biogeogr. 15, 200–212.

Azzali, S., Menenti, M., 2000. Mapping vegetation–soil–climate complexes in southern Africa using temporal Fourier analysis of NOAA-AVHRR NDVI data. Int. J. Remote Sens. 21 (5), 973–996.

Ayensu, E., Claasen, D.V., Collins, M., Dearing, A., Fresco, L., Gadgil, M., Gitay, H., Glaser, G., Lohn, C.L., Krebs, J., Lenton, R., Lubchenco, L., McNeely, J.A., Mooney, H.A., Pinstrup-Andersen, P., Ramos, M., Raven, P., Reid, W.V., Samper, C., Sarukhan, J., Schei, P., Tundisi, J.G., Watson, R.T., Xu, G.H., Zakri, A.H., 1999. Ecology – international ecosystem assessment. Science 286 (5440), 685–686.

Blanchet, F., Guillaume, Legendre, P., Borcard, D., 2008. Forward selection of explanatory variables. Ecology 89, 2623–2632.

Bradley, R., Jacob, J., Hermance, J.F., Mustard, 2007. A curve-fitting technique to derive inter-annual phonologies from time series of noisy NDVI satellite data. Remote Sens. Environ. 106, 137–145.

Breiman, L., Friedman, J.H., Olshen, R.A., Stone, C.J., 1984. Classification and Regression Trees. Chapman & Hall, ISBN: 0-412-04841-8.

Chen, X., Pan, W., 2002. Relationships among phenological growing season, time-integrated normalized difference vegetation index and climate forcing in the temperate region of eastern China. Int. J. Climatol. 22, 1781–1792.

Chen, X., Chengxin, X., Zhongjun, T., 2001. An analysis of relationships among plant community phenology and seasonal metrics of Normalized Difference Vegetation Index in the northern part of the monsoon region of China. Int. J. Biometeorol. 45, 170–177.

deBeurs, K.M., Henebry, G.M., 2004. Land surface phenology, climatic variation, and institutional change: analyzing agricultural land cover Change in Kazakhstan. Remote Sens. Environ. 89, 497–509.

Fensholt, R., Langanke, T., Rasmussen, K., Reenberg, A., Prince, S.D., Tucker, C.J., Scholes, R.J., Le, Q.G., Bondeau, A., Eastman, E., Epstein, H., Gaughan, A.E., Hellden, U., Mbow, C., Olsson, L., Paruelo, J., Schweitzer, C., Seaquist, J., Wessels, K., 2012. Greenness in semi-arid areas across the globe 1981–2007 – an earth observing satellite based analysis of trends and drivers. Remote Sens. Environ. 121, 144–158.

Graetz, R.D., 1989. Remote sensing of terrestrial ecosystem structure: an ecologist's pragmatic view. In: Hobbs, R.J., Mooney, H.A. (Eds.), Remote Sensing of Biosphere Functioning. Ecological Studies, vol. 79. Springer, New York, pp. 5–29.

Hellden, U., Tottrup, C., 2008. Regional desertification: a global synthesis. Global Planet. Change 64, 169–176.

Hill, J., Stellmes, M., Udelhoven, Th., Roder, A., Sommer, S., 2008. Mediterranean desertification and land degradation: mapping related land use change syndrimes based on satellite observations. Global Planet. Change 64, 146–157.

Hogda, K.A., Karlsen, S.R., Solheim, I., 2001. Climatic change impact on growing season in Fennoscandia studied by a time series of NOAA AVHRR NDVI data. In: Proceedings of IGARSS, 9–13 July 2001, Sydney, Australia, ISBN: 0-7803-7033-3.

Ivits, E., Cherlet, M., Tóth, G., Sommer, S., Mehl, W., Vogt, J., Micale, F., 2012. Combining satellite derived phenology with climate data for climate change impact assessment. Global Planet. Change, 88–89, 85–97.

Jolly, W.M., Running, S.W., 2004. Effect of precipitation and soil water potential on drought deciduous phenology in Kalahari. Global Change Biol. 10, 303–308.

Jeong, S.J., Ho, C.H., Park, T.W., Kim, J., Levis, S., 2011a. Impact of vegetation feedback on the temperature and its diurnal range over the Northern Hemisphere during summer in a 2 × CO_2 climate. Clim. Dyn., doi:10.1007./s00382-010-0827-x.

Jeong, S.J., Ho, C.H., Gim, H.J., Brown, M.E., 2011b. Phenology shifts at start vs. end of growing season in temperate vegetation over the Northern Hemisphere for the period 1982-2008. Global Change Biol. 17, 2385–2399, http://dx.doi.org/10.1111/j.1365-2486.2011.02397.x.

Jönsson, P., Eklundh, L., 2004. TIMESAT—a program for analyzing time-series of satellite sensor data. Comput. Geosci. 30, 833–845.
Julien, Y., Sobrino, J.A., 2009. Global land surface phenology trends from GIMMS database. Int. J. Remote Sens. 30 (13), 3495–3513.
Keeling, C.D., Chin, J.F.S., Whorf, T.P., 1996. Increased activity of Northern vegetation inferred from atmospheric CO_2 measurements. Nature 382, 146–149.
Lambin, E.F., Geist, H.J., 2006. Land use and land cover change. Local processes and global imoacts. In: Global Change – The IGBP Series. Springer Verlag, Berlin, Heidelberg, New York, 222 p.
Menzel, A., 2000. Trends in phenological phases in Europe between 1951 and 1996. Int. J. Biometeorol. 44, 76–81.
Metzger, M.J., Bunce, R.G.H., Jongman, R.H.G, 2011. Top-level tiers for Global Ecosystem Classification and Mapping Initiative (GEOSS Task ED-06-02). EBONE-WP3 Deliverable report D3.1.
Millenium Ecosystem Assessment, 2005. Ecosystems and Human Well Being: Synthesis. Island Press, Washington D.C.
Myneni, R.B., Keeling, C.D., Tucker, C.J., Asrar, G., Nemani, R.R., 1997. Increased plant growth in the northern high latitudes from 1981 to 1991. Nature 386, 698–702.
Nemani, R., Keeling, C.D., Hashimoto, H., Jolly, W.M., Piper, S.C., Tucker, C.J., Myneni, R., Running, W., 2003. Climate driven increases in global terrestrial net primary production from 1982–1999. Science 300, 1562–1563.
Paruelo, J.M., Jobbagy, E.G., Sala, O.E., 2001. Current distribution of ecosystem functional types in temperate South America. Ecosystems 4, 683–698.
Reed, B., Brown, J.F., Vanderzee, D., Loveland, T.R., Merchant, J.W., Ohlen, D.O., 1994. Measuring phenological variability from satellite imagery. J. Veg. Sci. 5, 703–714.
Schwartz, M.D., Reed, B.C., 1999. Surface phenology and satellite sensor-derived onset of greenness: an initial comparison. Int. J. Remote Sens. 20, 3451–3457.
Stöckli, R., Vidale, P.L., 2004. European plant phenology and climate as seen in a 20-year AVHRR land–surface parameter dataset. Int. J. Remote Sens. 25, 3303–3330.
Studer, S., Stöckli, R., Appenzeller, C., Vidale, P.L., 2007. A comparative study of satellite and ground-based phenology. Int. J. Biometeorol. 51 (5), 405–414.
Vitousek, P.M., Mooney, H.A., Luchenco, J., Melillo, J.M., 1997. Human domination of earth's ecosystems. Science 277, 494–499.
Wessels, K.J., prince, S.D., Malherbe, J., Small, J., Frost, P.E., VanZyl, D., 2007. Can human-induced land degradation be distinguished from the effects of rainfall variability? A case study in South Africa. J. Arid Environ. 68, 271–297.
Wessels, K., Steenkamp, K., vonMaltitz, G., Archibald, S., 2010. Remotely sensed vegetation phenology for describing and predicting the biomes of South Africa. Appl. Veg. Sci. II, 1–19, http://dx.doi.org/10.1111/j.1654-109X. 2010.01100.x.
White, M.A., Thomton, P.E., Running, S.W., 1997. A continental phenology model for monitoring vegetation responses to interannual climatic variability. Global Biogeochem. Cycl. 11 (2), 217–234.
Zaccarelli, N., Petrosillo, I., Zurlini, G. 2008. Retrospective analysis. In: Sven Erik Jørgensen, Brian D. Fath (Editor-in-Chief), Systems Ecology. Vol. 4 of Encyclopedia of Ecology, 5 vols. Oxford, Elsevier, pp. 3020–3029.
Zhang, X., Friedl, M.A., Schaaf, C.B., Strahler, A.H., Hodges, J.C.F., Gao, F., et al., 2003. Monitoring vegetation phenology using MODIS. Remote Sens. Environ. 84, 471–475.
Zhou, L., Tucker, C.J., Kaufmann, R.K., Slayback, D., Shabanov, N.V., Myneni, R.B., 2001. Variations in northern vegetation activity inferred from satellite data of vegetation index during 1981–1999. J. Geophys. Res. 106, 20069–20083.
Zhu, W., Tian, H., Xu, X., Pan, Y., Chen, G., Lin, W., 2011. Extension of the growing season due to delayed autumn over mid and high latitudes in North America during 1982-2006. Global Ecol. Biogeogr., http://dx.doi.org/10.1111/j.1466-8238.2011.00675.x.